ELSEVIER

Biophysical Chemistry 121 (2006) 163 – 170

Biophysical Chemistry

http://www.elsevier.com/locate/biophyschem

Mechanism of versatile peroxidase inactivation by Ca^{2+} depletion

Jorge Verdín [a], Rebecca Pogni [b], Alejandro Baeza [c], M. Camilla Baratto, Riccardo Basosi [b], Rafael Vázquez-Duhalt [a,*]

[a] *Institute of Biotechnology, UNAM, Av. Universidad 2001, Col. Chamilpa, Cuernavaca, Morelos 62250, Mexico*
[b] *Department of Chemistry, University of Siena, via Aldo Moro, 53100, Siena, Italy*
[c] *School of Chemistry, UNAM, Mexico, D.F. 04510, Mexico*

Received 7 December 2005; received in revised form 13 January 2006; accepted 16 January 2006
Available online 20 February 2006

Abstract

Versatile peroxidase (VP) from *Bjerkandera adusta*, as other class II peroxidases, is inactivated by Ca^{2+} depletion. In this work, the spectroscopic characterizations of Ca^{2+}-depleted VP at pH 4.5 (optimum for activity) and pH 7.5 are presented. Previous works on other ligninolytic peroxidases, such as lignin peroxidase and manganese peroxidase, have been performed at pH 7.5; nevertheless, at this pH these enzymes are inactive independently of their Ca^{2+} content. At pH 7.5, UV-Vis spectra indicate a heme-Fe^{3+} transition from 5-coordinated high-spin configuration in native peroxidase to 6-coordinated low-spin state in the inactive Ca^{2+}-depleted form. This Fe^{3+} hexa-coordination has been proposed as the origin of inactivation. However, our results at pH 4.5 show that Ca^{2+}-depleted enzyme has a high spin Fe^{3+}. EPR measurements on VP confirm the differences in the Fe^{3+} spin states at pH 4.5 and at 7.5 for both, native and Ca^{2+}-depleted enzymes. In addition, EPR spectra recorded after the addition of H_2O_2 to Ca^{2+}-depleted VP show the formation of compound I with the radical species delocalized on the porphyrin ring. The lack of radical delocalization on an amino acid residue exposed to solvent, W170, as determined in native enzyme at pH 4.5, explains the inability of Ca^{2+}-depleted VP to oxidize veratryl alcohol. These observations, in addition to a notorious redox potential decrease, suggest that Ca^{2+}-depleted versatile peroxidase is able to form the active intermediate compound I but its long range electron transfer has been disrupted.

Keywords: Calcium depletion; Inactivation; Versatile peroxidase

1. Introduction

Peroxidases catalyze the oxidation of substrates using H_2O_2 as a final electron acceptor. All peroxidases share the same catalytic mechanism consisting of three steps. First, the ground state ferric peroxidase reacts with H_2O_2 to yield a two electron-oxidized intermediate known as the compound I. Then, compound I is reduced by an exogenous substrate in a one-electron reaction to another enzyme intermediate called compound II, which is subsequently reduced back to the ground state by another substrate molecule also in an one-electron reaction [1].

Class II fungal peroxidases [2], such as lignin (LiP), manganese (MnP) and versatile (VP) peroxidases, are able to oxidize a wide range of substrates with high redox potential [3,4]. Despite their obvious biotechnological value, the application of peroxidases has been constrained by a low operational stability [5,6]. In addition to suicide inactivation suffered by all peroxidases [7,8], members of class II are also thermo-labile and pH sensitive [9,10]. Both in MnP and LiP, activity loss after thermal or alkaline treatment correlates with the release of the structural Ca^{2+} embedded in their structures [9,11,12]. These ions, referred to as the proximal and distal Ca^{2+}, act as structural stabilizers of the heme cavity [13–15]. In fact, they maintain the relative positions of proximal and distal

* Corresponding author. Tel.: +52 777 329 1655; fax: +52 777 317 2388.
E-mail address: vazqduh@ibt.unam.mx (R. Vázquez-Duhalt).

0301-4622/$ - see front matter © 2006 Elsevier B.V. All rights reserved.
doi:10.1016/j.bpc.2006.01.007

histidines, which are involved in the modulation of the peroxidase redox potential and in the acid–base activation of H_2O_2 at the beginning of the catalytic reaction, respectively [13].

Studies on the mechanism of alkaline and thermal inactivation of class II peroxidases have shown a change of the heme iron electronic state concomitant with structural calcium release. In native form, heme-Fe^{3+} mainly shows 5-coordinated high-spin (HS) configuration that changes to 6-coordinated low-spin (LS) state after inactivation. These observations, plus the inability of inactivated MnP to form compound I, have supported the bishistidine model of inactivation. This model argues that after Ca^{2+} release distal histidine becomes more flexible inducing a 6-coordinated heme-Fe^{3+}. Iron hexacoordination avoids the acid–base heterolysis of H_2O_2 leading to peroxidase inactivation [10,16,17]. However, it has been reported that heme-Fe^{3+} 6-coordination is not a deadlock, since it is easily reversed by iron chelating molecules [18]. More importantly, bishistidine inactivation model was built by characterizing Ca^{2+}-depleted MnP or LiP under conditions (pH 7.5 or higher) at which class II hemeperoxidases are not active independently of their Ca^{2+} content [16,17]. Alternatively, an important role has been proposed for the proximal histidine in the inactivation of horseradish peroxidase (HRP) [18], where structural changes have been detected around proximal cavity that could explain the decreased catalytic activity [18,19].

Versatile peroxidase (VP) is a structural and functional hybrid of LiP and MnP, showing both Mn^{2+}-dependent and Mn^{2+}-independent activities [20]. It has been isolated from several white rot fungi such as *Pleurotus eryngii* and *Bjerkandera adusta* [21,22]. In the present work, the spectroscopic and redox properties of the Ca^{2+} -depleted VP from *B. adusta* were studied at the catalytic pH in order to obtain further insight into the molecular causes of its inactivation.

2. Experimental

2.1. Chemicals

Bovine serum albumin (BSA), hydrogen peroxide, succinic acid, citric acid, potassium hydrogen phthalate, veratryl alcohol, anthracene, 9-methylanthracene, 2-methylanthracene, pyrene and tris(hydroxymethyl)aminomethane were provided by Sigma Chemical Co. (St. Louis, MO). Sodium phosphate, sodium chloride, potassium chloride, calcium chloride and EDTA were purchased from J.T. Baker (Phillipsburg, NJ). Perchloric acid was from Fluka Chemie (Switzerland). HPLC-grade acetonitrile was obtained from Fisher Scientific (Fairlawn, NJ).

2.2. Enzyme purification

Versatile peroxidase (M_r=36.6 kDa, pI=3.5, GenBank accession no. DQ060037) was isolated from *B. adusta* UAMH 8258 and purified by following the method of Wang [22]. The purity of the final VP preparation (R_Z=3.4) was confirmed by Coomassie stained 12% SDS-PAGE.

2.3. Activity assay

Mn^{2+}-independent activity, also referred as the ligninase activity, was measured spectrophotometrically as the formation of veratryl aldehyde at 310 nm (ε=9300 M^{-1} cm^{-1}) in reactions containing 4 mM veratryl alcohol in 50 mM succinic acid buffer, pH 3 [23]. The assay was started by the addition of H_2O_2 to a final concentration of 1 mM. Manganese-dependent activity was estimated by the H_2O_2-dependent formation of a Mn^{3+}-malonate complex at 270 nm (e=11590 M^{-1} cm^{-1}). Reactions contained 0.5 mM manganese sulfate in 50 mM malonate buffer (pH 4.5), and a final H_2O_2 concentration of 0.1 mM [24]. Protein concentration was determined by the Bradford method (Bio-Rad protein assay), using BSA as standard.

Oxidation of polycyclic aromatic hydrocarbons (anthracene, 2-methylanthracene, 9-methylanthracene and pyrene) was assayed in reaction mixtures containing 20 μM aromatic hydrocarbon, from 33 to 1400 nM VP and 10% (v/v) acetonitrile in 50 mM malonate buffer pH 4.5. Reactions were started by adding hydrogen peroxide to a final concentration of 1 mM and incubated during 10 min at room temperature. Enzyme activity was estimated as the decrease of aromatic compound measured by HPLC on a C_{18} reverse phase column (2.1×100 mm) Hypersil ODS 5 μ (Agilent) isocratically eluted (0.5 mL/min) with 70:30 v/v acetonitrile–water mixture. Substrates were monitored at 235 nm for pyrene, 250 nm for anthrecene and 2-methylanthracene, and at 255 nm for 9-methylanthracene.

2.4. Preparation and reconstitution of Ca^{2+}-depleted VP

Ca^{2+}-depleted peroxidase was prepared by incubating 12.94 μM VP in 12 mM Tris–HCl (pH 7.0) containing 9 mM EDTA until ligninase activity was not detected. Reconstitution was accomplished by dialyzing Ca^{2+}-depleted VP against 100 mM $CaCl_2$ in 20 mM Tris, pH 7.5 during 96 h at 4 °C.

The Ca^{2+} content of VP was determined by atomic absorption. Native and Ca^{2+}-depleted VP were exhaustively dialyzed against milliQ grade water and digested with perchloric acid. The digested samples were diluted in a solution containing 25 mM KCl, as ionization inhibitor, and 0.35% perchloric acid. Finally, atomic absorption measurements were performed on a Varian SpectrAA 220.

2.5. Electronic absorption spectroscopy

Absorption spectra of enzyme preparations were obtained in a Beckman DU650 spectrophotometer at 25 °C. The inactivated enzyme (Ca^{2+}-depleted) or native enzyme were dissolved in 50 mM citric acid, pH 4.5 and 50 mM Tris, pH 7.5 to a final concentration of 2.58 μM. The final pH of each solution was verified.

Soret band bleaching was monitored by UV-Vis spectrophotometry. After addition of 1 mM H_2O_2 to a Ca^{2+}-depleted VP preparation, spectra were acquired every 3 min. The inactivated enzyme (1.29 μM) was dissolved in 50 mM

Table 1
Dependence of VP catalytic activity on structural calcium ions

VP	Specific activity (%)[a]	Calcium content (Ca^{2+}/VP molecule)
Native	100	2.31 (±0.14)
Ca-depleted[b]	no activity	0.22 (±0.01)
Reconstituted[c]	40.83 (±0.88)	ND[d]

[a] Specific activity was measured by oxidation of veratryl alcohol and expressed as percentage of native VP.
[b] Calcium depletion was performed by incubating VP in 10 mM Tris, 7.5 mM EDTA, pH 7.0 at 25 °C until complete inactivation.
[c] For VP reconstitution, Ca^{2+}-depleted VP was dialyzed against 20 mM Tris, 0.1 M $CaCl_2$, pH 7.5 during 96 h at 4 °C.
[d] Not determined.

citric acid buffer solution (pH 4.5) or in a 50 mM Tris buffer (pH 7.5).

2.6. Redox potential

For redox potential measurements the concentration of native and Ca^{2+}-depleted VP was 78.68 μM. In both cases, the protein samples were dissolved in 50 mM citric acid buffer, pH 4.5. The working electrode was a platinum disc. A stainless steel bar was used as auxiliary electrode, while the reference electrode was a silver–silver chloride electrode. Ferro-ferricyanide (E=0.356 V/NHE) was utilized as internal reference.

2.7. Electron paramagnetic resonance spectroscopy

CW-X-band (9 GHz) EPR spectra of native and Ca^{2+}-depleted VP (0.14 mM) in 50 mM citric acid buffer at pH 4.5 and in 50 mM Tris buffer at pH 7.5 were obtained in a Bruker E500 Elexys Series using the Bruker ER 4122 SHQE cavity and an Oxford helium continuous flow cryostat (ESR900). Instrument settings are given in figure legends. The reaction of native and Ca^{2+}-depleted VP with H_2O_2, performed in a molar ratio enzyme/H_2O_2 of 1:8, was quickly stopped by immersion in liquid nitrogen before spectrum acquisition.

3. Results

Purified VP from *B. adusta* UAMH 8258, R_Z=3.4, was completely inactivated in the presence of EDTA (Table 1). As previously reported for MnP and LiP [9,11], activity loss correlates with a reduction in the calcium content of VP. This value diminishes from 2.31±0.14 Ca^{2+} ions per native VP molecule to only 0.22±0.01 Ca^{2+} ions per inactivated VP molecule (Table 1). Soret absorption band is preserved after EDTA treatment and Fe^{3+} remained coordinated to heme. The cause-consequence relationship between inactivation and Ca^{2+} loss was established by reconstituting the peroxidase activity in presence of $CaCl_2$. In our hands, the 40.83% of the original activity was recovered (Table 1), corroborating the direct dependence of catalytic activity on structural Ca^{2+} ions. Structural changes of some enzyme molecules during the Ca^{2+} extraction, protein washing and Ca^{2+} reincorporation may be the origin of the low activity recovery.

Activity pH profile was determined for both native and Ca^{2+}-depleted enzymes (data no shown). In both cases, the optimal pH was 4.5 and the profiles were essentially similar with a slight shift to the acidic side in the pH profile of Ca^{2+}-depleted VP.

Electronic absorption spectra for native and Ca^{2+}-depleted VP at both pH 7.5 (neutral) and pH 4.5 (catalytically optimum), are shown in Fig. 1. In previous studies, structural changes around heme cavity after Ca^{2+} loss were performed at pH 7.5 or higher [16,17]. However, fungal class II peroxidases, VP included, have atypically low optimal pH and, independently of Ca^{2+} content, they do not show catalytic activity at neutral pH [22,25]. Thus, the characterization of VP under conditions where normally it shows low catalytic performance (i.e., neutral pH) could lead to misinterpretation. At pH 7.5, native VP spectrum has characteristic bands at 588 nm (α), 541 nm (β) and 406.8 nm (Soret). Two charge transfer bands are also observed at 644.4 nm (CT1) and 498 nm (CT2). At pH 4.5, where the enzyme shows maximal Mn^{2+}-dependent activity [22], the spectrum of native protein is similar to that observed at pH 7.5, albeit CT1 band notoriously blue shifts to 635.2 nm,

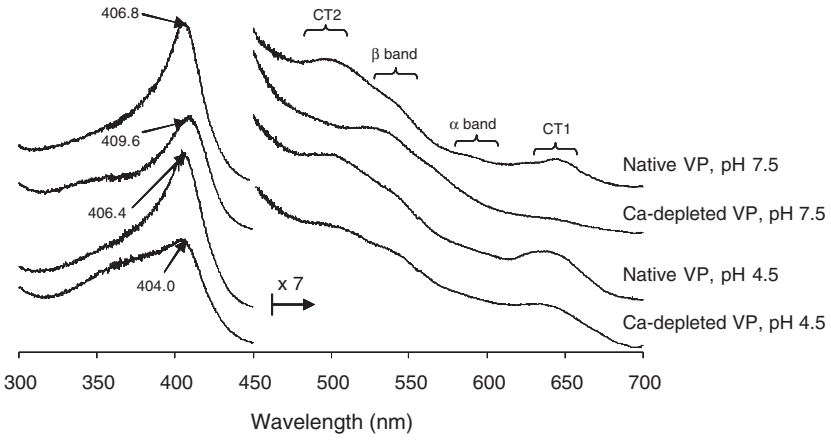

Fig. 1. Electronic absorption spectra of native and Ca^{2+}-depleted VP at two different pH (50 mM Tris, pH 7.5 and 50 mM sodium citrate, pH 4.5). For Ca^{2+}-depleted preparations, 12.94 μM VP from *B. adusta* was completely inactivated in 12 mM Tris, 9 mM EDTA, pH 7.0; prior to spectra acquisition, the inactivation mixture was five times diluted in the indicated buffer.

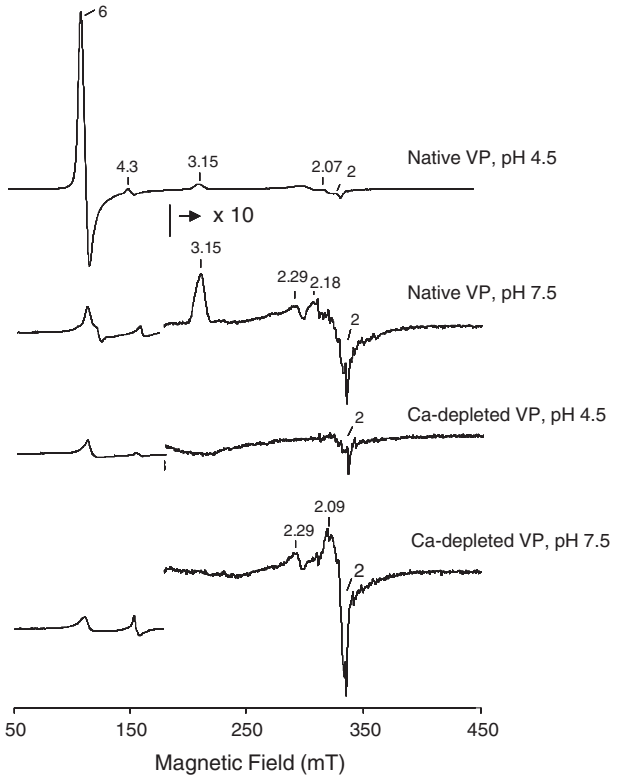

Fig. 2. Low temperature (20 K) EPR spectra of native and Ca^{2+}-depleted VP at two different pH (50 mM Tris, pH 7.5 and 50 mM sodium citrate, pH 4.5). The high field region has been amplified. All enzyme concentrations were 0.14 mM. Spectra were obtained at *v*, 9.39 GHz; modulation amplitude, 1 mT; microwave power, 2 mW and modulation frequency, 100 kHz.

indicating a heme iron 6-coordinate HS state (being H_2O the 6th ligand) upon pH acidification [26,27].

On the other hand, the spectrum of Ca^{2+}-depleted VP at pH 7.5 shows a notorious attenuation of the Soret band respect to native VP and the complete disappearance of both charge transfer (CT1, CT2) bands. Concomitantly, α and β bands appears enhanced and blue shifted to 563 and 523 nm, respectively. Furthermore, a new weak band is observed around 350 nm. The bands in the wavelength range 500–700 nm are very sensitive to structural changes around heme cavity, being CT1 band exclusive of HS peroxidases [27,28]. Vanishing of CT1 band in the spectrum of Ca^{2+}-depleted VP indicates the 6-coordinate LS configuration of heme-Fe^{3+}. From the characteristics of α and β bands can be inferred that a nitrogen atom, probably from distal histidine, acts as the sixth ligand [26,28]. Similar spectral features have been reported for MnP and LiP after inactivation treatments that involve the loss of structural Ca^{2+} ions. For these cases, bishistidine heme iron 6-coordination has been proposed as a barrier for acid–base heterolysis of H_2O_2, which would lead to peroxidase inactivation [10,16,17]. However, the spectrum of Ca^{2+}-depleted VP at pH 4.5 is not consistent with that observed at pH 7.5. Although they are weaker than native bands, the spectrum conserves CT1 and CT2 bands with maximum wavelength at 637.8 and 498 nm, respectively. The presence of CT1 band in Ca^{2+}-depleted VP spectrum indicates a HS configuration for heme-Fe^{3+} that opposes to bishistidine 6-coordinated LS observed for Ca^{2+}-free peroxidases at neutral pH. Soret band of Ca^{2+}-depleted VP at pH 4.5, unlike spectrum at pH 7.5, blue shifts to 404 nm and the shoulder at 350 nm absorbs more strongly. In addition, this strong absorption band at ~350 nm is also indicative of 5-coordinated HS state for iron [28].

The electronic configurations of native and Ca^{2+}-depleted VP at pH 4.5 and pH 7.5 were also assessed by low temperature Electron Paramagnetic Resonance, EPR (Fig. 2). Native VP at pH 4.5 shows a typical peroxidase EPR spectrum with mainly HS signals (g=6.00 and g=2.00) mixed with a low percentage of LS species (g=3.15, 2.07) [29,30]. The signal at g=4.3 corresponds to a non-heme rhombic Fe impurity [31]. At pH 7.5, the spectrum of native VP shows a marked decrease of the HS Fe species with a concomitant increase of the percentage of the LS Fe species. On the other hand, the Ca^{2+}-depleted enzyme spectrum at pH 4.5 is characterized by the absence of LS species, in agreement with the UV-Vis spectrum, albeit the high-spin ferric species ($g_{\perp}$=6.00 and $g_{\parallel}$=2.00) also decrease. At pH

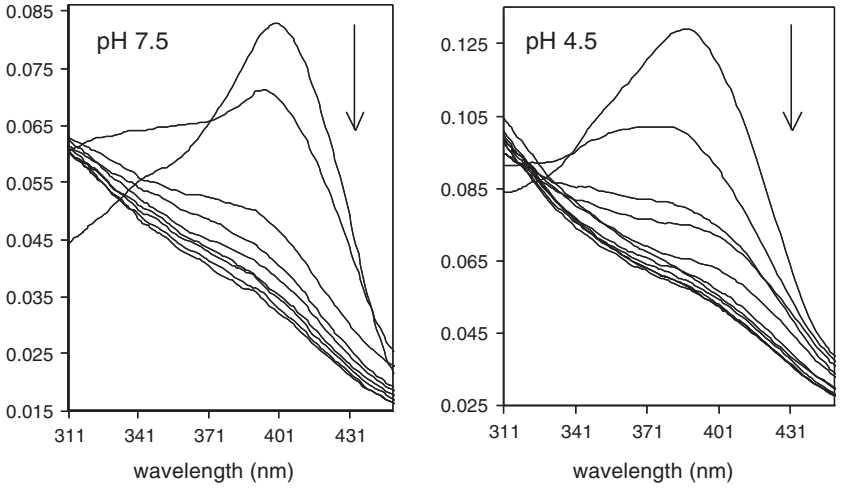

Fig. 3. Soret discoloration of 1.29 μM Ca^{2+}-depleted VP in the presence of 1 mM H_2O_2 at two different pH (50 mM Tris, pH 7.5 and 50 mM sodium citrate, pH 4.5). Spectra were obtained every 3 min at 25 °C. The arrow indicates the direction of change.

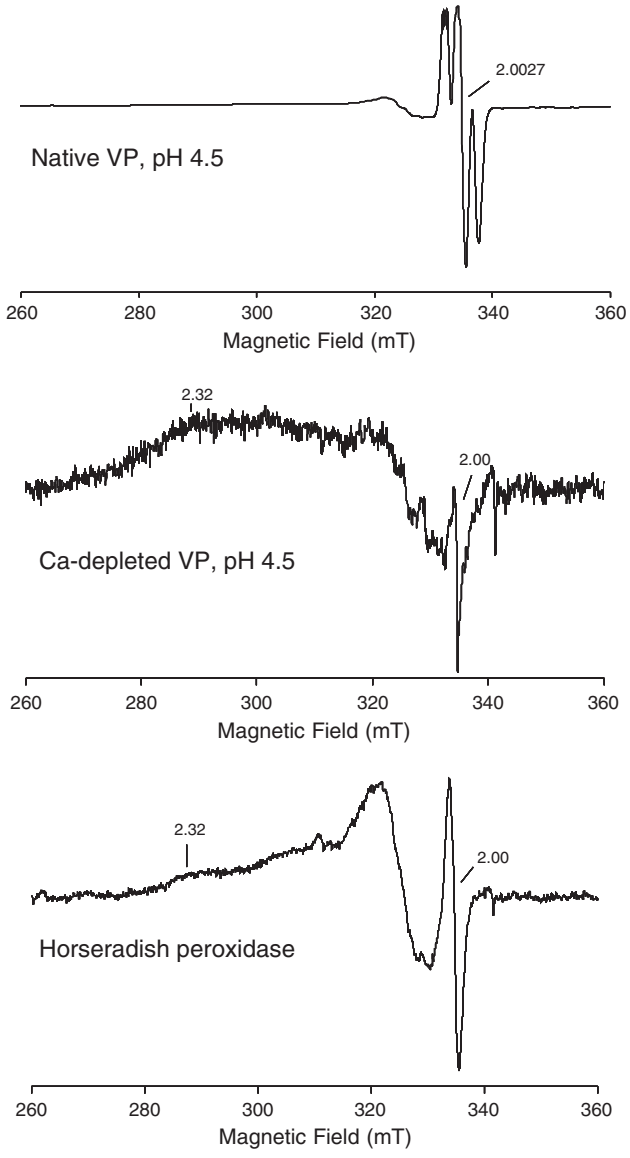

Fig. 4. Low temperature (20 K) EPR spectra of native VP (0.16 mM), Ca^{2+}-depleted VP (0.11 mM), and horseradish peroxidase (0.33 mM) after the addition of eight equivalents of H_2O_2 at pH 4.5. Instrument settings were: ν, 9.39 GHz; modulation amplitude, 0.2 mT; microwave power, 2 mW and modulation frequency, 100 kHz.

7.5, EPR spectrum of Ca^{2+}-depleted enzyme (Fig. 2) shows a decrease in the HS Fe species with a residual contribution of the LS Fe species, confirming the spectrophotometric measurements.

The thermal inactivation of LiP and MnP produces the loss of the distal Ca^{2+}, which may allow the movement of the α-helix containing distal His and its link to the iron forming a bishistidine arrangement [16,17]. As in our case, the EPR spectrum of a solution of Ca^{2+}-depleted MnP at pH 4.5 showed a decrease in the low-spin signal and a slight increase in the high-spin signal respect to that recorded at pH 7.5 [16]. It has been proposed that this pH-dependent transition at pH 4.5 is due to the protonation of distal His, which disrupts the direct link of distal His to the heme-Fe^{3+} and resulted in the formation of a complex with water bridged between the heme-Fe^{3+} and distal His [16]. This behavior confirms our results obtained for Ca^{2+}-depleted VP at pH 4.5.

Soret band of Ca^{2+}-depleted VP was discolored in the presence of 1 mM H_2O_2 at both pH 7.5 and 4.5 (Fig. 3). Hemeperoxidases undergo autocatalytic oxidative inactivation in the presence of excess H_2O_2 and in the absence of a reducing substrate due to the formation of deleterious compound III [32]. This superoxo-Fe^{3+} porphyrin radical arises from the reaction of compound II with H_2O_2 [33]. The degradation of the heme prosthetic group is one of the molecular events occurring during this mechanism-based inactivation [7,8]. At pH 4.5, as expected for a HS penta-coordinated Fe, Ca^{2+}-depleted VP is able to react with the hydrogen peroxide molecule. On the other hand, the heme destruction of 6-coordinated LS state Ca^{2+}-depleted VP at pH 7.5 indicates that H_2O_2 is able to disrupt the interaction between the distal histidine and the heme-Fe^{3+} and reacts to form the deleterious species that produce oxidative inactivation, even if it is unable to react with an exogenous reducing substrate. On the basis of these observations, it is possible to deduce that VP inactivation does not rise from the impossibility to react with H_2O_2, even in the case of a LS 6-coordinate electronic configuration, but from a mechanism directly related with the oxidation of exogenous substrates.

EPR measurements of the reaction of Ca^{2+}-depleted VP with hydrogen peroxide were performed for deeper analysis. Spectra were recorded after the addition of a small excess of hydrogen peroxide (1 : 8 enzyme : H_2O_2 molar ratio) in order to prime the catalytic cycle but to prevent the oxidative inactivation. Fig. 4 shows EPR radical spectra of native and Ca^{2+}-depleted VP and compared with these obtained from horseradish peroxidase. As previously reported [29], EPR radical spectrum of native VP at pH 4.5 and after the addition of 8 equivalents of H_2O_2 showed the formation of a tryptophan radical with a g_{iso} value of 2.0027. This radical has been shown to be essential for veratryl alcohol oxidation [34]. On the other hand, Ca^{2+}-depleted VP spectrum at pH 4.5 is significantly different to the native protein (Fig. 4), showing signals with $g_{\|}$=2.3 and $g_{\perp}$ ~2.00 values. Similar radical signals have been obtained for the Ca^{2+}-depleted VP at pH 7.5 (data not shown). This spectrum is compared with these from native horseradish peroxidase obtained in the same experimental conditions (Fig. 4). The signals with $g_{\|}$=2.3 and $g_{\perp}$~2.00 are perfectly overlapping. These results suggest that the radical species formed in Ca^{2+}-depleted VP seems to be a

Table 2
Specific activity of native and Ca^{2+}-depleted versatile peroxidase on different substrates

Substrate	Native VP (min^{-1})	Ca^{2+}-depleted VP (min^{-1})
Mn^{2+}	1142 (±91)	53 (±4)
Veratryl alcohol	251 (±20)	No activity
ABTS [a]	178 (±17)	13 (±1)
DEPDA [b]	64497 (±6 213)	3000 (±554)
Guaiacol	237 (±4)	18 (±2)

[a] 2′2-Azino-bis(3-ethylbenzothiazoline-6-sulfonic acid.
[b] *N*,*N*-diethyl-1-phenylenediamine sulfate.

Table 3
Specific activity for native and Ca^{2+}-depleted versatile peroxidase on polycyclic aromatic hydrocarbons with different ionization potentials

Substrate	Ionization potential (eV)[a]	Specific activity (min^{-1})	
		Native VP	Ca-depleted VP
9-Methylanthracene	7.23	296.86 (±15.91)[b]	0.58 (±0.05)
2-Methylanthracene	7.42	22.08 (±1.99)	NAD[c]
Anthracene	7.55	8.37 (±0.42)	NAD
Pyrene	7.72	3.85 (±0.57)	NAD

Reaction mixture contained 20 μM aromatic compound and 10% acetonitrile in 50 mM malonic acid buffer, pH 4.5.
[a] Values obtained from Ref. [37].
[b] Values in parentheses are standard deviations.
[c] NAD, no activity detected.

porphyrin-based radical, as in Compound I, instead of Trp radical like was shown for the native enzyme [29,30].

Native and Ca^{2+}-depleted VP were assayed on different substrates (Table 2). Ca^{2+}-depleted VP is able to oxidize Mn^{2+} to Mn^{3+} and shows between 4.6% and 7.7% of the native activity with some organic substrates. However no veratryl alcohol oxidation was detected. In native VP, tryptophan radical formation is coupled to compound I and compound II reductions and W170 residue is essential for veratryl alcohol oxidation [34], while Mn^{2+} is oxidized at the heme edge. This intramolecular reaction is possible because tryptophan oxidation proclivity is combined with the high redox potential of heme catalytic intermediates. With the aim of verify whether the inability to oxidize superficial Trp in Ca^{2+}-depleted VP arises from an oxidizing power decrease, redox potentials for the couple Fe^{3+}/Fe^{2+} of native and Ca^{2+}-depleted VP were determined. At pH 4.5 native VP has a redox potential of 390 mV, while Ca^{2+}-depleted sample showed a lower value of 190 mV. On the other hand, the activity profile against different polycyclic aromatic hydrocarbons with a wide range of ionization potentials were determined for native and Ca^{2+}-depleted VP (Table 3). In concordance with its low ionization potential, 9-methylanthracene was preferentially oxidized by native VP followed by 2-methylanthracene, anthracene and pyrene. On the other hand, Ca^{2+}-depleted VP, with a lower redox potential and a reduced catalytic activity, only was able to oxidize the easiest oxidizing substrate, 9-methylanthracene. These data confirm the reaction of Ca^{2+}-depleted VP with H_2O_2 and the activation of the catalytic cycle. Moreover, the reduction of the oxidizing power of Ca^{2+}-depleted VP, indicated by the reduction of the redox potential and the constriction of the ionization potential range of substrates, could be the origin of the inability to form the tryptophan based radical, essential for veratryl alcohol oxidation, and in general, its inability to oxidize high ionization potential substrates.

4. Discussion

The catalytic activity of versatile peroxidase from *B. adusta*, as other peroxidases, depends on Ca^{2+} ions embedded into the enzyme (Table 1). Calcium release has been also observed during the thermal and alkaline inactivations of MnP and LiP, while HRP partially loses its catalytic activity upon Ca^{2+} depletion [9–11,35]. Previous inactivation model proposed an increase in distal histidine flexibility after Ca^{2+} loss, leading a 6-coordinating heme-Fe^{3+} and to an activity inhibition [16,17]. In addition, Howes et al. [18] suggested, for Ca^{2+}-depleted HRP, other structural changes around proximal histidine that could also influence the catalytic performance of the enzyme. Unfortunately, most analogous precedent studies were performed at neutral pH condition [16,17], while at pH 4.5 VP shows its maximum catalytic activity [22].

We have found significant differences in the iron spin state according the pH in both, native and Ca^{2+}-depleted VP (Figs. 1 and 2). Electronic absorption spectra at pH 7.5 indicate a 6-coordinated LS electronic configuration for Ca^{2+}-depleted VP, as supported by the vanishing of CT1 band as well as the shift and intensity enhancement of α and β bands respect to native VP (Fig. 1) [28]. Under these experimental conditions, equivalent spectral features were observed for thermally inactivated MnP and LiP, being interpreted to be the result of heme-Fe^{3+} bishistidine 6-coordination [16,17]. In such electronic state, heme-Fe^{3+} was believed unable to utilize H_2O_2 in order to form compound I. Nevertheless, Ca^{2+}-depleted VP can react with H_2O_2 leading to compound III and Soret band discoloration (Fig. 3), the characteristic signal of the suicide inactivation of peroxidases [7,8], which contradicts the bishistidine-driven catalytic deadlock. In fact, the disruption of the distal Fe-histidine bond by heme-Fe^{3+} chelating compounds have been easily accomplished in HRP [18], indicating that the strength of distal histidine-Fe bond is not enough to avoid H_2O_2 activation.

However, the HS configuration of Ca^{2+}-depleted VP at pH 4.5, indicated by the CT1 electronic absorption band at 637.8 nm (Fig. 1) and EPR signals at $g=6.00$ and $g=2.00$ (Fig. 2), confirms that VP inactivation is independent of bishistidine heme-Fe^{3+} hexa-coordination. The dependence of electronic absorption spectrum on the pH was also reported for Ca^{2+}-depleted MnP [16]. It is reasonable to suppose that calcium depletion actually promotes a greater flexibility of heme cavity, including the distal histidine, and under specific pH conditions is able to 6-coordinate heme-Fe^{3+}. However, as described before, distal Fe-imidazole bond may reduce, but not block, the VP catalytic activity.

Redox potential of hemeperoxidases is controlled by the relative position and the strength of the imidazolate character of proximal histidine, which are both modulated by a series of H-bonds to neighbour residues and by the proximal Ca^{2+} [13,36,37]. The redox potential for the pair Fe^{3+}/Fe^{2+} of Ca^{2+}-depleted VP is lower than the native enzyme, indicating structural changes in the proximal cavity that could increase the imidazolate character of proximal histidine by modifying its H-bonding pattern or, alternatively, by changing the bond distance between proximal histidine and heme-Fe^{3+}. Although the couple Fe^{3+}/Fe^{2+} is not involved in the catalytic reaction of peroxidases, redox potential changes with the same trend could be expected for the pairs compound I/compound II and compound II/ground state in the catalytic cycle [37]. Thus, the observed low activity of Ca^{2+}-depleted VP could be related

with a reduced oxidizing power. In agreement, class I peroxidases, which do not contain structural calcium ions, show low redox potentials due to shorter proximal Fe-imidazole bond [13]. This effect has also been observed in Ca^{2+}-depleted horseradish peroxidase, where there are structural changes around proximal histidine and the concomitant change of the redox potential [18,19]. In support of this, the catalytic profile of VP after Ca^{2+} depletion shows a notorious reduction, being only able to oxidize substrates with low ionization potentials (Table 3). It is well known that the specific activity of lignin peroxidase [3,38], manganese peroxidase [39] and chloroperoxidase [40] is inversely proportional to the ionization potential of the substrate (polycyclic aromatic hydrocarbons). Because redox potential limits the range of substrates that peroxidases can oxidize, its reduction promotes a drop in the peroxidase catalytic capabilities.

Reaction of Ca^{2+}-depleted VP with H_2O_2 produces a radical that remains delocalized on the porphyrin ring, corresponding to compound I intermediate (Fig. 4). Contrasting, under the same conditions, native VP shows a solvent exposed tryptophan radical (Fig. 4), which has been assigned to the Trp170 [29]. During catalytic cycle, this solvent exposed residue is selectively oxidized by compound I and compound II in order that the peroxidase oxidizing power becomes accessible for substrates unable to reach the heme edge [13,34]. Nevertheless, the decrease of the oxidizing capability of VP after calcium depletion prevents the oxidation of W170. In this way, the lack of the tryptophanyl radical in Ca^{2+}-depleted VP abolishes the catalytic activity mediated by such radical.

So far we can conclude that the low activity of Ca^{2+}-depleted VP obeys to structural changes that alter their oxidizing capabilities. These changes seem to prevent the oxidation of substrates with high ionization potential and the oxidation of the superficial W170, which is essential for the veratryl alcohol oxidation. Even if is unable to react with some endogenous substrates, compound I intermediate of Ca^{2+}-depleted VP is able to support the self-oxidative heme destruction, as well as the oxidation of low-potential substrates. Thus, structural calcium ions have a relevant role in versatile peroxidase from *B. adusta*, which is reflected in the catalytic properties of the enzyme.

Acknowledgements

We thank Raunel Tinoco, Rosa Román and Pilar Fernández for technical support. We thank Stefania Giansanti for valuable contribution. J.V. holds a CONACYT (144892) and UNAM (DGEP) fellowships. This work was funded by the National Council for Science and Technology of Mexico.

References

[1] H.B. Dunford, Heme Peroxidases, VHC-Wiley, New York, 1999.
[2] K.G. Welinder, Superfamily of plant, fungal and bacterial peroxidases, Curr. Opin. Struck. Biol. 2 (1992) 388–393.
[3] R. Vazquez-Duhalt, D.W.S. Westlake, P. Fedorak, Lignin peroxidase oxidation of aromatic compounds in systems containing organic solvents, Appl. Environ. Microbiol. 60 (1994) 459–466.
[4] D. Wesenberg, I. Kyriakides, S.N. Agathos, White-rot fungi and their enzymes for the treatment of industrial dye effluents, Biotechnol. Adv. 22 (2003) 161–187.
[5] S. Colonna, N. Gaggero, C. Richelmi, P. Pasta, Recent biotechnological developments in the use of peroxidases, TIBTECH 17 (1999) 163–168.
[6] F. van de Velde, F. van Rantwijk, R.A. Sheldon, Improving the catalytic performance of peroxidases in organic synthesis, Trends Biotech. 19 (2001) 73–80.
[7] H. Jenzer, W. Jones, H. Kohler, On the molecular mechanism of lactoperoxidase-catalyzed H_2O_2 metabolism and irreversible enzyme inactivation, J. Biol. Chem. 261 (1986) 15550–15556.
[8] B. Valderrama, M. Ayala, R. Vazquez-Duhalt, Suicide inactivation of peroxidases and the challenge of engineering more robust enzymes, Chem. Biol. 9 (2002) 555–565.
[9] G.R.J. Sutherland, S.D. Aust, The effects of calcium on the thermal stability and activity of manganese peroxidase, Arch. Biochem. Biophys. 332 (1996) 128–134.
[10] P. George, M. Kvaratskhelia, M.J. Dilworth, R.N.F. Thorneley, Reversible alkaline inactivation of lignin peroxidase involves the release of both the distal and proximal site calcium ions and bishistidine co-ordination of the haem, Biochem. J. 344 (1999) 237–244.
[11] G. Nie, S.D. Aust, Effect of calcium on the reversible thermal inactivation of lignin peroxidase, Arch. Biochem. Biophys. 337 (1997) 225–231.
[12] S.L. Timofeevski, S.D. Aust, Kinetics of calcium release from manganese peroxidase during thermal inactivation, Arch. Biochem. Biophys. 342 (1997) 169–175.
[13] T. Choinowski, W. Blodig, K.H. Winterhalter, K. Piontek, The crystal structure of lignin peroxidase at 1.7 Å resolution reveals a hydroxy group on the C-Beta of tryptophan 171: a novel radical site formed during the redox cycle, J. Mol. Biol. 286 (1999) 809–827.
[14] M. Sundaramoorthy, K. Kishi, M.H. Gold, T.L. Poulos, The crystal structure of manganese peroxidase from *Phanerochaete chrysosporium* at 2.06 Å resolution, J. Biol. Chem. 269 (1994) 32759–32767.
[15] M. Gajhede, D.J. Schuller, A. Henriksen, A.T. Smith, T.L. Poulos, Crystal structure of horseradish peroxidase C at 2.15 Å resolution, Nat. Struct. Biol. 4 (1997) 1032–1038.
[16] G.R.J. Sutherland, L. Schick Zapanta, M. Tien, S.D. Aust, Role of calcium in maintaining the heme environment of manganese peroxidase, Biochemistry 36 (1997) 3654–3662.
[17] G. Nie, S.D. Aust, Spectral changes of lignin peroxidase during reversible inactivation, Biochemistry 36 (1997) 5113–5119.
[18] B.D. Howes, A. Feis, L. Raimondi, C. Indiani, G. Smulevich, The critical role of the proximal calcium ion in the structural properties of horseradish peroxidase, J. Biol. Chem. 276 (2001) 40704–40711.
[19] Y. Shiro, M. Kurono, I. Morishima, Presence of endogenous calcium ion and its functional and structural regulation in horseradish peroxidase, J. Biol. Chem. 261 (1986) 9382–9390.
[20] A.T. Martínez, Molecular biology and structure-function of lignin-degrading heme peroxidases, Enzyme Microbiol. Technol. 30 (2002) 425–444.
[21] F.J. Ruiz-Dueñas, S. Camarero, M. Pérez-Boada, M.J. Martínez, A.T. Martínez, A new versatile peroxidase from *Pleurotus*, Biochem. Soc. Trans. 29 (2001) 116–122.
[22] Y. Wang, R. Vazquez-Duhalt, M.A. Pickard, Purification, characterization, and chemical modification of manganese peroxidase from *Bjerkandera adusta* UAMH 8258, Curr. Microbiol. 45 (2002) 77–87.
[23] M. Tien, T.K. Kirk, Lignin Peroxidase of *Phanerochaete chrysosporium*, Methods Enzymol. 161 (1988) 238–248.
[24] H. Wariishi, H.B. Dunford, I.D. MacDonald, M.H. Gold, Manganese peroxidase from the lignin-degrading basidiomycete *Phanerochaete chrysosporium*, J. Biol. Chem. 264 (1989) 3335–3340.
[25] M. Tien, T.K. Kirk, C. Bull, J.A. Fee, Steady-state and transient-state kinetic studies on the oxidation of 3,4-dimethoxybenzyl alcohol catalyzed by the ligninase of *Phanerochaete chrysosporium* Burds, J. Biol. Chem. 261 (1986) 1687–1693.
[26] G. Smulevich, M.A. Miller, J. Kraut, T.G. Spiro, Conformational change and histidine control of heme chemistry in cytochrome c peroxidase:

resonance Raman evidence from Leu-52 and Gly-181 mutants of cytochrome c peroxidase, Biochemistry 30 (1991) 9546–9558.
[27] G. Smulevich, F. Neri, M.P. Marzocchi, K.G. Welinder, Versatility of heme coordination demonstrated in a fungal peroxidase. Absorption and resonance Raman studies of *Coprinus cinereus* peroxidase and the Asp245: Asn mutant at various pH values, Biochemistry 35 (1996) 10576–10585.
[28] G. Smulevich, Understanding heme cavity structure of peroxidases: comparison of electronic absorption and resonance Raman spectra with crystallographic results, Biospectroscopy 4 (1998) S3–S17.
[29] R. Pogni, M.C. Baratto, S. Giansanti, C. Teutloff, J. Verdin, B. Valderrama, F. Lendzian, W. Lubitz, R. Vazquez-Duhalt, R. Basosi, Tryptophan-based radical in the catalytic mechanism of versatile peroxidase from *Bjerkandera adusta*, Biochemistry 44 (2005) 4267–4274.
[30] A. Ivancich, G. Mazza, A. Desbois, Comparative electron paramagnetic resonance study of radical intermediates in turnip peroxidase isozymes, Biochemistry 40 (2001) 6860–6866.
[31] W.E. Blumberg, J. Peisach, A. Wittenberg, J.B. Wittenberg, The electronic structure of protoheme peroxidases: I. An electron paramagnetic resonance and optical study of herseradish peroxidase and its derivatives, J. Biol. Chem. 243 (1968) 1854–1862.
[32] M.B. Arnao, M. Acosta, J.A. del Rio, R. Varon, F. Garcia-Canovas, A kinetic study on the suicide inactivation of peroxidase by hydrogen peroxide, Biochim. Biophys. Acta 1041 (1990) 43–47.
[33] H. Wariishi, M.H. Gold, Lignin peroxidase compound: III. Mechanism of formation and decomposition, J. Biol. Chem. 265 (1990) 2070–2077.
[34] M. Pérez-Boada, F.J. Ruiz-Dueñas, R. Pogni, R. Basosi, T. Choinowski, M.J. Martínez, K. Piontek, A.T. Martínez, Versatile peroxidase oxidation of high redox potential aromatic compounds: site-directed mutagenesis, spectroscopic and crystallographic investigation of three long-range electron transfer pathways, J. Mol. Biol. 354 (2005) 385–402.
[35] R.H. Haschke, J.M. Friedhoff, Calcium-related properties of horseradish peroxidase, Biochem. Biophys. Res. Commun. 80 (1978) 1039–1042.
[36] L. Banci, I. Bertini, P. Turano, M. Tien, T.K. Kirk, Proton NMR investigation into the basis for the relatively high redox potential of lignin peroxidase, Proc. Natl. Acad. Sci. U. S. A. 88 (1991) 6956–6960.
[37] C.D. Millis, D. Cai, M.T. Stankovich, M. Tien, Oxidation-reduction potentials and ionization states of extracellular peroxidases from the lignin-degrading fungus *Phanerochaete chrysosporium*, Biochemistry 28 (1989) 8484–8489.
[38] K.E. Hammel, B. Kalyanaraman, T.K. Kirk, Oxidation of polycyclic aromatic hydrocarbons and dibenzo(p)dioxins by *Phanerochaete chrysosporium* ligninase, J. Biol. Chem. 261 (1986) 16948–16952.
[39] B.W. Bogan, R.T. Lamar, K.E. Hammel, Fluorene oxidation in vivo by *Phanerochaete chrysosporium* and in vitro during manganese peroxidase-dependent lipid peroxidation, Appl. Environ. Microbiol. 62 (1996) 1788–1792.
[40] R. Vazquez-Duhalt, M. Ayala, F.J. Marquez-Rocha, Biocatalytic chlorination of aromatic hydrocarbons by chloroperoxidase of *Caldariomyces fumago*, Phytochemistry 58 (2001) 929–933.